Published in final edited form as:

J Invest Dermatol. 2019 March ; 139(3): 552–561. doi:10.1016/j.jid.2018.09.028.

Chemoprotective effects of dietary grape powder on ultraviolet B radiation-mediated skin carcinogenesis in SKH-1 hairless mice

Chandra K. Singh[*,1], **Charlotte A. Mintie**[*,1], **Mary A. Ndiaye**[1], **Gagan Chhabra**[1], **Panshak P. Dakup**[2], **Ting Ye**[3], **Menggang Yu**[4], and **Nihal Ahmad**[1,5]

[1] Department of Dermatology, University of Wisconsin, Madison, Wisconsin, 53706, USA

[2] Department of Pharmaceutical Sciences, College of Pharmacy and Pharmaceutical Sciences, Washington State University, Spokane, WA, 99202, USA

[3] Department of Statistics, University of Wisconsin, Madison, Wisconsin 53706, USA

[4] Department of Biostatistics & Medical Informatics, University of Wisconsin, Madison, WI, 53792, USA

[5] William S. Middleton VA Medical Center, Madison, Wisconsin, 53705, USA

Abstract

Skin cancer is the most frequently diagnosed cancer in the US, and solar ultraviolet (UV) radiation is an established causative factor for ~90% of these cases. Despite efforts aimed at UV protection, including use of sunscreen and clothing, annual cases of skin cancers continue to rise. Here, we report that dietary grape powder (GP) mitigates UVB-mediated skin carcinogenesis in SKH-1 hairless mouse model. Employing a UVB initiation-promotion protocol, where mice were exposed to 180 mJ/cm^2 UVB 2x/week for 28 weeks, we determined the effects of GP-fortified diet (3% or 5%) on skin carcinogenesis. GP consumption at both doses resulted in marked inhibition in tumor incidence, as well as a delay in onset of tumorigenesis. Molecular analyses of skin and tumor tissue demonstrated that GP-mediated protective response against UVB-induced skin cancer was accompanied by enhanced DNA damage repair, reduced proliferation, increased apoptosis and modulations in several oxidative stress markers specifically related to inhibition of oxidative stress and increased ROS metabolism. Interestingly, NRF2, an activator of cellular antioxidant response, was decreased by GP feeding, suggesting a supportive role in tumor cell survival. Overall, our study suggested that dietary grape, containing several antioxidants in natural amalgamation, may protect against UVB-mediated skin carcinogenesis.

Keywords

Grape; Non-melanoma skin cancers; chemoprevention

Correspondence to: Nihal Ahmad, Ph.D., Department of Dermatology, University of Wisconsin, Medical Sciences Center, 1300 University Avenue, Madison, Wisconsin, 53706, Phone: (608) 263-2532; Fax: (608) 263-5223; nahmad@wisc.edu.

[*]Contributed equally

CONFLICT OF INTEREST

The authors state no conflict of interest.

INTRODUCTION

Nonmelanoma skin cancers (NMSCs) are the most commonly diagnosed malignancy, affecting more than 3.5 million Americans on an annual basis (Rogers et al., 2015). NMSCs are mostly comprised of basal cell carcinomas (BCCs) and squamous cell carcinomas (SCCs), which arise in the epidermis from keratinocytes that have undergone malignant transformation (Bowden, 2004). Solar ultraviolet (UV) radiation is believed to be the most prevalent natural carcinogen in our environment and has been identified as a causative factor for ~90% of NMSC cases (Mancebo and Wang, 2014). Solar UV radiation that penetrates the atmosphere is mainly comprised of UVA (90–99%; 320–400 nm) and UVB (1–10%; 290–320 nm), whereas most of the higher energy UV radiation (UVC; 200–290 nm) is absorbed by stratospheric ozone and other atmospheric components (Chhabra et al., 2017). Preventing skin damage from UV radiation is largely done through regular and ample application of sunscreen, seeking shade, and wearing clothing that covers the skin. However, continuously rising numbers of skin cancer cases suggest that implementation of these measures has not been fully effective. Interestingly, prior skin cancer history has been linked to an increased risk of developing other neoplasms (Kahn et al., 1998; Levi et al., 1998; Rogers et al., 2015). Additionally, according to the most recent estimates, NMSC has a $4.8 billion annual burden on the US economy (Guy Jr et al., 2015). All these reasons provide a rationale to intensify our efforts towards the identification of additional approaches for skin cancer chemoprevention.

Using naturally occurring antioxidants has practical implications in reducing cancer risk because unlike carcinogenic environmental factors that are difficult to control, individuals can make decisions to modify their choices of food and beverages they consume. The grape antioxidant resveratrol (3,5,4′-trihydroxystilbene) is one such agent that has been studied at length for its health-promoting and anticancer effects (Aziz et al., 2005; Singh et al., 2015b). However, the grape itself is a natural conglomeration of more than 1600 compounds that also includes quercetin, melatonin, lycopene and several other potent antioxidants (Pezzuto, 2008; Singh et al., 2016). Recent studies indicate that these compounds may help protect against certain cancers, heart disease, nerve and brain disorders, arthritis and an array of other conditions (reviewed in (Singh et al., 2015a)). Because of the high antioxidant capacity of many of these constituents and their natural combination in grapes, we reasoned that dietary grapes, containing a number of useful food components, could be very useful against UVB-mediated skin carcinogenesis. We believe that the whole food concept, which relies on additive and synergistic response of multiple agents, is a better option for cancer chemoprevention. This study was undertaken to determine the protective effects and potential mechanisms of grape powder-fortified diet on UVB-induced skin cancer in SKH-1 hairless mice, a relevant model for skin carcinogenesis (Benavides et al., 2009).

RESULTS & DISCUSSION

Dietary grape powder (GP) decreases skin tumor incidence and delays onset of tumorigenesis in SKH-1 hairless mouse model of skin carcinogenesis

Since UV exposure, especially the UVB spectrum is a major risk factor for skin cancer, this study was designed to access the effects of dietary GP feeding on UVB exposure mediated

skin tumorigenesis in mice. The details of the major compounds of GP (obtained from the California Table Grape Commission (CTGC)) are presented in Figure 1a. As laid out in Figure 1b, we determined the effects of dietary GP in a long-term, chronic UVB-mediated skin carcinogenesis model in SKH-1 hairless mice that closely mimics human skin photocarcinogenesis (de Gruijl and Forbes, 1995; Kligman and Kligman, 1981). We found that GP supplementation was well tolerated by the mice, and average diet consumption/mouse/day corresponded to 102 and 180 mg of GP consumption by 3% and 5% GP supplemented groups, respectively. These correspond to human equivalent doses of 24.77 and 43.61 g/day, using the dose translation model proposed in (Reagan-Shaw et al., 2008), or 1.07 and 1.85 servings of grapes, respectively.

During the study, mice developed different sized tumors, as shown in Figure 1c. Details about the tumor multiplicity data of weeks 24–27 showing the significant differences in tumor incidence, especially in 5% GP, are presented in Figure 1d. Small papules started appearing at 10, 14, and 13 weeks of treatment in control, 3%, and 5% GP mice, respectively (Figure 2a). Our statistical model of the observed reduction in tumor incidence indicated that the overall group effects of the fitted results are not significant; however, the time effect is borderline significant with a p-value of 0.0506 (Figure 2a), indicating the weekly tumor incidence is increasing over time. Survival analysis indicated no significant difference in the onset of tumors, with median survival without appearance of papules at 15 weeks (control and 5% GP) and 17 weeks (3% GP) (Figure 2b). Both GP groups demonstrated reduced tumor volume by week 26 (Figure 2c). By week 28, average tumor volume was markedly reduced in 3% GP (23.35±6.34 mm^3) and 5% GP (15.36±2.90 mm^3) from control (92.1±50.89 mm^3); however, the fitted results indicate that the group and time effects from 3% and 5% GP feeds are not significant. At the time of euthanasia, final counts (multiplicity) of discernable papules (<2 mm) were taken as an independent measure and, along with large tumors (>2 mm), were recorded and analyzed. Our data suggested a marked reduction of both small and large tumors, and 5% GP was found to cause a significant decrease (p-value 0.021) in smaller tumors (Figure 2d). Interestingly for several of the tumor parameters analyzed (Figures 1c–d and 2a–d), the effects of 3% and 5% GP treatments did not considerably differ, leading us to conclude that the chemoprotective response of GP is similar at both the tested doses.

Dietary GP reduces UVB-mediated DNA damages and decreases epidermal thickening

UVB causes direct DNA damage via formation of mutagenic/carcinogenic cyclobutane pyrimidine dimers (CPDs) and 6–4 photoproducts (6–4 PPs) (Bowden, 2004). Under normal conditions, nucleotide excision repair (NER) removes 6–4 PP and CPDs after probing the genome for helix distortions. However, CPDs are poorly recognized and repair can be ineffective. These dimers result in the transcription of C→T or CC→TT UVB signature mutations (de Gruijl, 1999; Ichihashi et al., 2003; Mancebo and Wang, 2014) found in multiple tumor-related genes, including tumor suppressor *p53*, a gene mutated in ~90% of human SCCs (Agar et al., 2004) and up to 100% in SKH-1 mouse (Melnikova et al., 2005). Moreover, it has been shown that CPDs may cause NMSC tumorigenesis (Jans et al., 2005). To determine the effect of GP on the repair of UVB photoproducts, epidermal genomic DNA was isolated from the harvested skin and photoproduct damage was measured by slot blot.

As demonstrated in Figures 3a–b, we found a significant reduction in CPD levels in the involved (adjacent to tumors, with UV exposure) skin of the 5% GP group, and a trend of reduced CPDs in the un-involved (stomach skin, no UV exposure) skin. Collectively, the reduction of CPDs remaining in the skin 3–5 days after UVB exposure suggests that there is likely enhanced NER capacity in mouse skin epidermis with GP consumption since NER is the sole mechanism for the repair of CPDs and (6–4) PPs in mice and humans (Dakup and Gaddameedhi, 2017; Gaddameedhi et al., 2011). Our assay was not able to detect (6–4) PPs, potentially due to their shorter half-life (data not shown). No CPDs were detected in normal skin samples from a separate cohort of untreated mice that had no UV exposure (Supplementary Figure S1).

Due to the fact that epidermal keratinocytes are at a high risk of UVB-induced damages, the epidermal thickness was determined as a measure of keratinocyte proliferation (Hassan et al., 2015). Representative images of H&E stained skin are shown in Figure 3c. Measurement of the epidermal thickness using ImageJ showed a trend towards reduced thickness with GP supplementation, although statistical significance was not attained (Figure 3d). This could also be due to chronic UV exposure protocol used in our experiments, especially since epidermal hyperplasia is mostly seen as a result of acute UV exposure.

Chemoprotective response of dietary GP was associated with decreased proliferation and increased apoptosis in UVB-induced tumors

We next determined the effect of GP feeding on the expression of the proliferation marker proliferating cell nuclear antigen (PCNA), a protein that is not only involved in many cellular functions, including DNA replication and repair (Moldovan et al., 2007), but also can serve as an indirect indicator of UVB-induced damage (Moore et al., 2004). We found reduced expression of PCNA at mRNA and protein levels in both the 3% and 5% GP groups (Figures 4a–b). Additionally, analysis of Ki-67, a classic marker for proliferating cells that is often regarded as having prognostic significance in many neoplasms (Koseoglu et al., 2009; Scholzen and Gerdes, 2000), demonstrated the similar trend (Figures 4c–d), indicating decreased cellular proliferation in the tumor tissue of the GP-supplemented mice.

One of the key hallmarks of cancer is the ability of cells to escape apoptosis. Therefore, we evaluated the effects of GP on the apoptosis markers. Utilizing the Caspase-Glo 3/7 assay, which measures executioner caspase-3 and −7 activities, we observed a trend towards increased mean relative intensity in 5% GP tumors as compared to control tumors (Figure 4e). To explore this further, we determined the effect of GP feeding on caspases-3 and −7 proteins using immunoblot analyses. Although we found no significant change in caspase-3 (data not shown), we found a marked increase in the levels of cleaved caspase-7 (Figure 4f) in both 3% and 5% GP groups, though the increase appeared higher in the 3% GP group. Further, caspase-7 has been shown to cleave poly (ADP-ribose) polymerase (PARP), a protein whose cleavage facilitates cellular disassembly and indicates that cells are undergoing apoptosis (Boucher et al., 2012). Immunoblot analysis revealed an increase in the levels of cleaved PARP in tumor tissues of GP-supplemented mice, suggesting an enhanced apoptosis by GP feeding (Figure 4g). Further, evaluation of the pro-survival protein BCL-2, which is known to be differentially expressed in various malignancies and

considered as a useful prognostic biomarker (Thomadaki and Scorilas, 2006), demonstrated downregulation in the GP supplemented groups (Figure 4h). Collectively, these observations suggest that GP decreases proliferation and increases apoptosis of tumor cells, contributing to reduced tumor incidence and volume.

Chemoprotective effects of dietary GP were associated with modulation of oxidative stress marker 4-hydroxynonenal (4-HNE), independent of nuclear factor erythroid 2–related factor 2 (NRF2)

UV radiation has been shown to induce reactive oxygen species (ROS) in skin (Heck et al., 2003). Although the skin contains elaborate antioxidant defense mechanisms, excessive ROS can lead to oxidative stress in skin. To evaluate the effect of GP on oxidative stress, we assessed the lipid peroxidation biomarker 4-HNE and oxidative stress response marker NRF2. 4-HNE accumulates during oxidative stress due to ROS attack on the polyunsaturated fatty acid chain of the lipid membrane, leading to severe cell damage (Mylonas and Kouretas, 1999). As shown in Figures 5a–b, a marked decrease in the accumulation of 4-HNE was found in the tumors of both groups of GP-supplemented mice. Interestingly, NRF2, an activator of the cellular antioxidant response, was also found to be decreased in the tumor samples of GP-supplemented mice (Figures 5c–d). Traditionally, it is thought that NRF2 signaling quenches ROS, leading to repair of oxidative damage. However, NRF2 has been found to be dysregulated in many cancers, and in many cases has constitutive activation resulting in higher proliferation rates and tumorigenicity (Rojo de la Vega et al., 2018), suggesting that increased NRF2 expression is contributing to a pro-survival environment in the tumor.

Dietary GP significantly alters multiple oxidative stress genes and pathways

In an attempt to uncover other genes or pathways associated with oxidative stress and antioxidants that may be modulated by GP supplementation, we used a commercially available oxidative stress PCR array profiling the expression of 84 key genes related to oxidative stress. Details of the expression analyses are presented in Supplementary Table S1–S2 and Supplementary Figure S2. We found that out of 84 genes tested, 13 were upregulated and 3 were downregulated significantly by ≥1.75-fold change in 5% GP, and ≥1.4-fold change in 3% GP (Figure 6a). The expression of these 16 genes was validated using RT-qPCR assay (Figure 6b). Upregulated genes included antioxidant gene *Srxn1*, glutathione peroxidase *Gpx7*, peroxiredoxins *Prdx2, 4, 5* and *6*, peroxidase *Ptgs2*, genes involved in superoxide metabolism *Cyba* and *Nox4*, oxidative stress-responsive genes *Ccl5, Gss and Hmox*, and the oxygen transporter *Vim*. Downregulated genes included *Ucp2*, a gene known to be involved in superoxide metabolism, and the oxidative stress-responsive genes (*Ercc2* and *Gclc*). However, only 5 genes were found to be significantly modulated during validation (*Ccl5, Cyba, Gpx7, Nox4,* and *Pxdx5*). All others were found with similar trends to the array but were not statistically significant. All the validated genes, except *Prdx5*, are known to be involved in ROS metabolism. *Ccl5* and *Gpx7* are known to act as oxidative stress response genes, while *Cyba* and *Nox4* are involved in superoxide metabolism. *Cyba* encodes p22(phox) protein, which is known to be involved in superoxide production and phagocytosis (Stasia, 2016). Interestingly, p22(phox) partners with NADPH oxidases (Noxs), including *Nox4*, to generate superoxide intracellularly (Stasia, 2016). *Gpx7*

is the only member of the glutathione peroxidase (GPx) family without any GPx activity, although it is an important oxidative stress sensor and has been found to suppress ROS and protect against oxidative DNA damage (Chen et al., 2016). *Prdx5* is an antioxidant gene that codes for a mitochondrial peroxiredoxin, which is known to play an important role in cell protection against oxidative stress by detoxifying peroxides and as a sensor of hydrogen peroxide-mediated signaling events (Knoops et al., 2011).

To further analyze the gene-gene interactions, the 16 significantly modulated genes obtained from PCR array were uploaded into IPA software to identify networks of interacting genes. IPA suggested links to other genes with potential involvement in antioxidant functions, resulting in a network. Interestingly, all of the identified network genes were found to have links to cancer (shown with a pink boundary in Figure 6c). Additionally, the potential involvement of other important genes such as *Erk1/2, P38 Mapk, Tgfβ, Ap1* and *Hsp27* were identified by IPA, as they were not part of the PCR array. Analysis of cumulative gene functions predicted that GP supplementation inhibits oxidative stress and the quantity of ROS, while increasing the metabolism of ROS (Figure 6d).

Collectively, our data suggested that GP-supplementation imparts a marked chemoprotective response against UVB exposure-mediated skin carcinogenesis in SKH-1 mice via multiple molecular mechanisms, as it affects DNA damage repair, cell proliferation, apoptosis and oxidative stress pathways (Figure 6e). Moreover, the observed effects appear to occur by modulating genes involved in antioxidant function, metabolism of ROS, superoxide metabolism and/or oxidative stress-response. The chemoprotective effects of dietary GP observed in this study are in accordance with our earlier investigation, where we showed that the topical application of the grape antioxidant resveratrol resulted in a significant inhibition in tumor incidence and delay in the onset of tumorigenesis (Aziz et al., 2005). Additionally, in another study, though not related to UVB-induced skin cancer, GP was shown to inhibit chemically-induced skin carcinogenesis in SENCAR mice (Hanausek et al., 2011). This study also evaluated the effects of other grape constituents and found that similar to GP, resveratrol, quercetin and grape seed extract containing proanthocyanidin B-2-gallate, inhibited the 7,12-dimethylbenz[a]anthracene (DMBA)-induced epidermal hyperplasia, proliferation, and inflammation.

A limited number of studies have suggested reasonable pharmacokinetics profile of grape polyphenol following consumption of grape constituents. One such study looked at oral supplementation of a standardized grape polyphenol mixture (consisting of grape seed extract, concord grape juice and resveratrol) to Zucker diabetic fatty rats. The authors found definite bioavailability of polyphenol metabolites, with C_{max} between 1–3 hours, which then declined by 8 hours (Chen et al., 2017). Additionally, because of the promising health effects of grape and grape constituents, few human clinical trials have been performed in the recent past (reviewed in (Singh et al., 2015a)). One study evaluating postprandial hydrophilic plasma antioxidant capacity (AOC) after GP intake in 6 women found significantly increased AOC suggesting that GP consumption can maintain a redox balance from the free radicals that occur during carbohydrate metabolism (Prior et al., 2007). These studies suggest that the oral grape consumption can provide a systemic distribution of its various constituents, capable of imparting health-promoting effects.

As the cases of NMSC continue to rise, it is imperative to find chemoprotective measures to prevent damages caused by UV radiation. Natural dietary agents, including grapes, offer us beneficial antioxidants and other phytonutrients, which can enrich our diets and lead to better health. In this *in vivo* study, we demonstrated that dietary grape powder afforded protection against UVB-induced damages that lead to skin carcinogenesis, as evidenced by increased DNA damage repair, reduced cell proliferation and oxidative stress, and enhanced apoptotic response and ROS metabolism. These findings suggest that ingestion of antioxidant-rich GP may lead to decreased tumorigenesis of NMSC in humans and that inclusion of 1–2 daily servings of grapes may be beneficial for a healthy lifestyle. However, further investigation is required to validate our findings and to develop strategies for skin cancer management using grapes.

MATERIALS AND METHODS

Dietary grape feed

Freeze-dried grape powder (GP), composed of fresh red, green, and black grapes (*Vitis vinifera*) of both seeded and seedless varieties was obtained from the CTGC. This mixture is a representative of the mix of grapes available to consumers in the U.S. during the 9-month long California grape season, typically between July and October. For GP production, grapes were frozen, ground on dry ice, freeze-dried, then re-ground to preserve the integrity of the biologically active compounds. For our studies, we used GP from a single batch made in 2011, which was incorporated into AIN-76A diet by Envigo (Madison, WI) at concentrations of 0, 3, or 5% GP. All diets were matched to the natural sugar content of the 5% GP diet.

UVB-mediated skin carcinogenesis model of SKH-1 hairless mice.

The animal experiments were approved by the University of Wisconsin (UW) Institutional Animal Care and Use Committee. SKH-1 hairless mice (female, 5 weeks old, n=12 per group) were obtained from Charles River Laboratories (Wilmington, MA) and allowed to acclimatize for one week prior to study initiation. Animals had access to water and feed *ad libitum*. The experimental diets (containing 0, 3, or 5% GP) were started beginning on day one of UV exposure and continued until the termination of the experiment. Throughout the experiment, animals were closely monitored for general health, body weight, and food consumption. Measured doses of UVB irradiation were administered using a calibrated Research Irradiator (Daavlin Company, Bryan, OH). All animals received UVB exposures twice weekly at 180 mJ/cm^2 starting at 6 weeks of age and continuing for 28 weeks. "Dosing holidays," where one UV dose was purposefully skipped, happened during weeks 8, 10, and 18, due to noticeably high amounts of erythema. Mice were examined for tumors before each UVB exposure. Distinguishable tumors (initially arising as papules) were counted weekly up to 27 weeks, as well as at time of euthanasia, and tumor measurements using a digital caliper were started upon reaching at least 2 mm in diameter. Tumor volume was calculated using the formula length × width × height × (π / 6). At the termination of the experiment, mice were euthanized 3–5 days after their last UV exposure and skin and tumor tissue were collected for further analysis.

Tissue embedding, epidermal thickness evaluation and immunohistology

Harvested tumors, adjacent (involved) skin, and non-UV treated (un-involved) stomach skin were formalin fixed, paraffin embedded, sectioned, and mounted on serial slides at the UW Carbone Cancer Center Experimental Pathology Core Laboratory. One serial slide from each mouse was stained with hematoxylin and eosin (H&E) and analyzed for epidermal thickness as described in Supplementary Information online. All other immunostaining and imaging were performed as described in Supplementary Information online.

Preparation of epidermal gDNA and immuno-slot blot analysis

Epidermal gDNA was isolated from involved and un-involved skin from 5 randomly selected animals in the control and 5% GP groups. The quality and quantity of the gDNA were assessed using a NanoDrop 2000 spectrophotometer (Thermo Fisher Scientific) before measurement of photoproducts by immuno-slot blot analysis as previously reported (Gaddameedhi et al., 2010). Details are provided in Supplementary Information online.

Tissue lysate preparation, immunoblot analysis, and RT-qPCR

Liquid nitrogen flash-frozen tumors were ground into powder using a mortar and pestle in liquid nitrogen before being divided for protein and RNA analysis. Equal amounts of protein or RNA from 3 mice from each experimental group were pooled for subsequent studies, with 3 separate groupings made to represent averages of the entire cohort. Immunoblotting and RT-qPCR were performed using standard techniques, detailed in Supplementary Information online. Details of antibodies and primers used are also provided in Supplementary Tables S3 and S4, respectively, in Supplementary Information online.

Oxidative stress PCR array and Ingenuity Pathway Analysis (IPA)

The effects of GP feeding on oxidative stress and antioxidant response genes were assessed using the Qiagen Mouse Oxidative Stress RT2 Profiler™ PCR Array (#PAMM-065Z) per manufacturer's instructions. Resultant Ct values were uploaded to the Qiagen GeneGlobe Data Analysis Center and analyzed using *Gapdh* and *Actb* reference genes (Supplementary Tables S1–S2). Selected genes from the PCR array results were validated using RT-qPCR analysis. Primer pairs detailed in Supplementary Table S4 were retrieved from Primer Bank (Wang et al., 2012). Further, to understand the pathways affected by GP supplementation, differentially expressed genes from the PCR array were analyzed by Qiagen's IPA software using genes that showed a fold-changes of ≥1.75 in 5% GP and ≥1.4-fold in 3% GP. Full details are provided in Supplementary Information online.

Caspase-Glo 3/7 Assay

Protein lysates were prepared as described in Supplementary Information online, and the Caspase-Glo 3/7 Assay (Promega) was used per the manufacturer's protocol.

Statistical analysis

Statistical support for tumor data was provided by the collaborating statistics core facility statisticians (TY and MY). One mouse from the control group developed lymphoma at week 21 and therefore euthanized early and excluded from analysis. Weekly tumor incidence and

mean tumor volume measurements were analyzed by a mixed effect model $Y_{ij} = \mu_0 + \mu_1 I(G_i = 2) + \mu_2 I(G_i = 3) + \beta t_j + b_{i,0} + b_{i,1} t_j + \varepsilon_{ij}$, where G_i is the group indicator, which equals 1, 2, and 3 for the control, 3% GP, and 5% GP feed groups, respectively. The 'fixed' effect parameters μ_0, μ_1, μ_2, β represent the underlying population average effect, $b_{i,0}$, $b_{i,1}$ are subject-specific random effects, and ε_{ij} is the error or noise term. Intuitively, the time effect is modeled linearly for every subject, but the intercept and slope of the linear time trend can deviate from the population average. Due to the skew in tumor counts, a small number was added to every tumor to ensure a positive value. The data was log transformed and treated as the response variable. Tumor-free survival was defined as the time (in weeks) until tumor development. Because all mice developed tumors, no censoring was needed; therefore, Dunn's Kruskal-Wallis multiple comparisons test was performed to examine the treatment effects, with the p-value adjusted using the Benjamini-Hochberg method. Note that Dunn's test is non-parametric, leaving no assumption on the distribution. At the time of euthanasia, the treatment effects with respect to the final counts (multiplicity) of discernable papules (<2 mm) and large tumors (>2 mm) are estimated by fitting linear regression model $Y_i = \mu_0 + \mu_1(G_i = 2) + \mu_2 I(G_i = 3) + \varepsilon_i$, respectively, where Y_i is the log tumor count. All other statistical analyses were performed using GraphPad PRISM 5.0 software (GraphPad Software, La Jolla, CA).

Supplementary Material

Refer to Web version on PubMed Central for supplementary material.

ACKNOWLEDGMENTS

This work was partially supported by funding from the California Table Grape Commission (CTGC), as well as the NIH (grant numbers R01AR059130 and R01CA176748 to NA), and the Department of Veterans Affairs (VA Merit Review Award I01CX001441; and a Research Career Scientist Award IK6BX003780 to NA). We also acknowledge the core facilities supported by the Skin Diseases Research Center (SDRC) Core Grant P30AR066524 from NIH/NIAMS. Use of the Experimental Pathology Laboratory and Biostatistics Shared Resource are supported through the UW Carbone Cancer Center Support Grant P30 CA014520.

REFERENCES

Agar NS, Halliday GM, Barnetson RS, Ananthaswamy HN, Wheeler M, Jones AM. The basal layer in human squamous tumors harbors more UVA than UVB fingerprint mutations: A role for UVA in human skin carcinogenesis. Proc Natl Acad Sci U S A 2004;101:4954–59. [PubMed: 15041750]

Aziz MH, Reagan-Shaw S, Wu J, Longley BJ, Ahmad N. Chemoprevention of skin cancer by grape constituent resveratrol: relevance to human disease? FASEB J 2005;19:1193–5. [PubMed: 15837718]

Benavides F, Oberyszyn TM, VanBuskirk AM, Reeve VE, Kusewitt DF. The hairless mouse in skin research. J Dermatol Sci 2009;53:10–18. [PubMed: 18938063]

Boucher D, Blais V, Denault JB. Caspase-7 uses an exosite to promote poly(ADP ribose) polymerase 1 proteolysis. Proc Natl Acad Sci U S A 2012;109:5669–74. [PubMed: 22451931]

Bowden GT. Prevention of non-melanoma skin cancer by targeting ultraviolet-B-light signalling. Nat Rev Cancer 2004;4:23–35. [PubMed: 14681688]

Chen TY, Ferruzzi MG, Wu QL, Simon JE, Talcott ST, Wang J, et al. Influence of diabetes on plasma pharmacokinetics and brain bioavailability of grape polyphenols and their phase II metabolites in the Zucker diabetic fatty rat. Mol Nutr Food Res 2017;61.

Chen YI, Wei PC, Hsu JL, Su FY, Lee WH. NPGPx (GPx7): a novel oxidative stress sensor/transmitter with multiple roles in redox homeostasis. Am J Transl Res 2016;8:1626–40. [PubMed: 27186289]

Chhabra G, Ndiaye MA, Garcia-Peterson LM, Ahmad N. Melanoma Chemoprevention: Current Status and Future Prospects. Photochem Photobiol 2017;93:975–89. [PubMed: 28295364]

Dakup P, Gaddameedhi S. Impact of the Circadian Clock on UV-Induced DNA Damage Response and Photocarcinogenesis. Photochem Photobiol 2017;93:296–303. [PubMed: 27861965]

de Gruijl FR. Skin cancer and solar UV radiation. Eur J Cancer 1999;35:2003–09. [PubMed: 10711242]

de Gruijl FR, Forbes PD. UV-induced skin cancer in a hairless mouse model. BioEssays 1995;17:651–60. [PubMed: 7646487]

Gaddameedhi S, Kemp MG, Reardon JT, Shields JM, Smith-Roe SL, Kaufmann WK, et al. Similar nucleotide excision repair capacity in melanocytes and melanoma cells. Cancer Res 2010;70:4922–30. [PubMed: 20501836]

Gaddameedhi S, Selby CP, Kaufmann WK, Smart RC, Sancar A. Control of skin cancer by the circadian rhythm. Proc Natl Acad Sci U S A 2011;108:18790–5. [PubMed: 22025708]

Guy GP Jr, Machlin SR, Ekwueme DU, Yabroff KR. Prevalence and Costs of Skin Cancer Treatment in the U.S., 2002−2006 and 2007−2011. Am J Prev Med 2015;48:183–87. [PubMed: 25442229]

Hanausek M, Spears E, Walaszek Z, Kowalczyk MC, Kowalczyk P, Wendel C, et al. Inhibition of Murine Skin Carcinogenesis by Freeze-Dried Grape Powder and Other Grape-Derived Major Antioxidants. Nutr Cancer 2011;63:28–38. [PubMed: 21108125]

Hassan SMA, Hussein AJ, Saeed AK. Role of green tea in reducing epidermal thickness upon ultraviolet light-B injury in BALB/C mice. Adv Biol 2015;890632:1–6

Heck DE, Vetrano AM, Mariano TM, Laskin JD. UVB light stimulates production of reactive oxygen species: unexpected role for catalase. J Biol Chem 2003;278:22432–6. [PubMed: 12730222]

Ichihashi M, Ueda M, Budiyanto A, Bito T, Oka M, Fukunaga M, et al. UV-induced skin damage. Toxicology 2003;189:21–39. [PubMed: 12821280]

Jans J, Schul W, Sert Y-G, Rijksen Y, Rebel H, Eker APM, et al. Powerful Skin Cancer Protection by a CPD-Photolyase Transgene. Curr Biol 2005;15:105–15. [PubMed: 15668165]

Kahn HS, Tatham LM, Patel AV, Thun MJ, Heath CW Jr. Increased cancer mortality following a history of nonmelanoma skin cancer. JAMA 1998;280:910–2. [PubMed: 9739976]

Kligman LH, Kligman AM. Histogenesis and progression in ultraviolet light-induced tumors in hairless mice. J Natl Cancer Inst 1981;67:1289–93. [PubMed: 6947111]

Knoops B, Goemaere J, Van der Eecken V, Declercq JP. Peroxiredoxin 5: structure, mechanism, and function of the mammalian atypical 2-Cys peroxiredoxin. Antioxid Redox Signal 2011;15:817–29. [PubMed: 20977338]

Koseoglu RD, Sezer E, Eyibilen A, Aladag İ, Etikan İ. Expressions of p53, cyclinD1 and histopathological features in basal cell carcinomas. J Cutan Pathol 2009;36:958–65. [PubMed: 19187116]

Levi F, La Vecchia C, Te VC, Randimbison L, Erler G. Incidence of invasive cancers following basal cell skin cancer. Am J Epidemiol 1998;147:722–6. [PubMed: 9554413]

Mancebo SE, Wang SQ. Skin cancer: role of ultraviolet radiation in carcinogenesis. Rev Environ Health 2014;29:265–73. [PubMed: 25252745]

Melnikova VO, Pacifico A, Chimenti S, Peris K, Ananthaswamy HN. Fate of UVB-induced p53 mutations in SKH-hr1 mouse skin after discontinuation of irradiation: relationship to skin cancer development. Oncogene 2005;24:7055–63. [PubMed: 16007135]

Moldovan G-L, Pfander B, Jentsch S. PCNA, the Maestro of the Replication Fork. Cell 2007;129:665–79. [PubMed: 17512402]

Moore JO, Palep SR, Saladi RN, Gao D, Wang Y, Phelps RG, et al. Effects of ultraviolet B exposure on the expression of proliferating cell nuclear antigen in murine skin. Photochem Photobiol 2004;80:587–95. [PubMed: 15623348]

Mylonas C, Kouretas D. Lipid peroxidation and tissue damage. In Vivo 1999;13:295–309. [PubMed: 10459507]

Pezzuto JM. Grapes and human health: a perspective. J Agric Food Chem 2008;56:6777–84. [PubMed: 18662007]

Prior RL, Gu L, Wu X, Jacob RA, Sotoudeh G, Kader AA, et al. Plasma antioxidant capacity changes following a meal as a measure of the ability of a food to alter in vivo antioxidant status. J Am Coll Nutr 2007;26:170–81. [PubMed: 17536129]

Reagan-Shaw S, Nihal M, Ahmad N. Dose translation from animal to human studies revisited. FASEB J 2008;22:659–61. [PubMed: 17942826]

Rogers HW, Weinstock MA, Feldman SR, Coldiron BM. Incidence Estimate of Nonmelanoma Skin Cancer (Keratinocyte Carcinomas) in the U.S. Population, 2012. JAMA Dermatol 2015;151:1081–6. [PubMed: 25928283]

Rojo de la Vega M, Chapman E, Zhang DD. NRF2 and the Hallmarks of Cancer. Cancer Cell 2018;34:21–43. [PubMed: 29731393]

Scholzen T, Gerdes J. The Ki-67 protein: From the known and the unknown. J Cell Physiol 2000;182:311–22. [PubMed: 10653597]

Singh CK, Liu X, Ahmad N. Resveratrol, in its natural combination in whole grape, for health promotion and disease management. Ann N Y Acad Sci 2015a;1348:150–60. [PubMed: 26099945]

Singh CK, Ndiaye MA, Ahmad N. Resveratrol and cancer: Challenges for clinical translation. Biochim Biophys Acta 2015b;1852:1178–85. [PubMed: 25446990]

Singh CK, Siddiqui IA, El-Abd S, Mukhtar H, Ahmad N. Combination chemoprevention with grape antioxidants. Mol Nutr Food Res 2016;60:1406–15. [PubMed: 26829056]

Stasia MJ. CYBA encoding p22(phox), the cytochrome b558 alpha polypeptide: gene structure, expression, role and physiopathology. Gene 2016;586:27–35. [PubMed: 27048830]

Thomadaki H, Scorilas A. BCL2 family of apoptosis-related genes: functions and clinical implications in cancer. Crit Rev Clin Lab Sci 2006;43:1–67. [PubMed: 16531274]

Wang X, Spandidos A, Wang H, Seed B. PrimerBank: a PCR primer database for quantitative gene expression analysis, 2012 update. Nucleic Acids Res 2012;40:D1144–9. [PubMed: 22086960]

a

Major Compounds in Grape Powder	Concentration (mg/kg GP) ±SD
Catechins	
Catechin	19.59 ± 1.06
Epicatechin	8.77 ± 0.71
Anthocyanins	
Peonidin	148.75 ± 8.19
Cyanidin	20.1 ± 1.33
Malvidin	127.77 ± 8.33
Flavonols	
Kaempferol	1.03 ± 0.16
Isorhamnetin	1.06 ± 0.11
Quercetin	14.44 ± 1.20
Taxifolin	1.87 ± 0.10
Stilbenes	
Resveratrol	0.85 ± 0.16
Total Polyphenols (in gallic acid equivalents)	3260

b

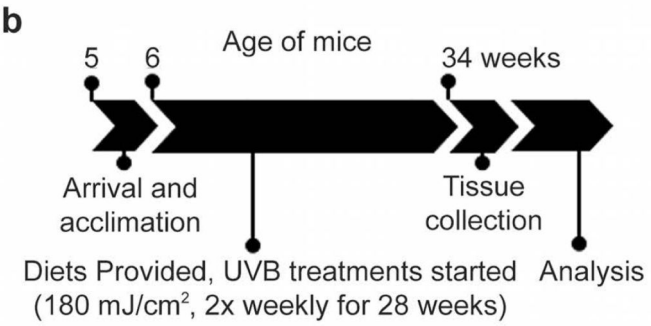

c

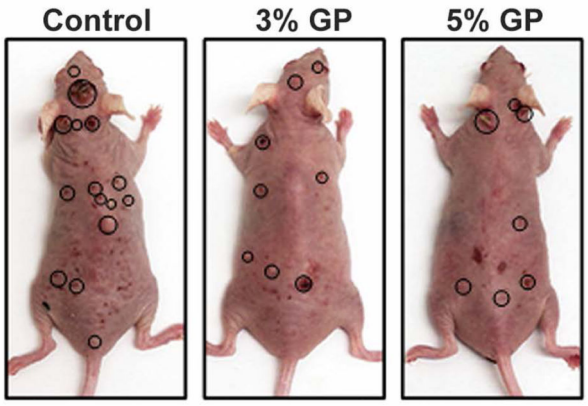

d

	Control n=11			3% GP n=12				5% GP n=12			
Tumor multiplicity at:	Total tumors /group	Tumor mean	SEM	Total tumors /group	Tumor mean	SEM	p-value	Total tumors /group	Tumor mean	SEM	p-value
Week 24	215	19.5	2.1	175	14.6	1.7	0.0408	166	13.8	1.0	0.0198
Week 25	221	20.1	2.2	183	15.3	1.9	0.0595	171	14.3	1.1	0.0247
Week 26	306	27.8	3.9	271	22.6	1.8	0.1744	240	20.0	2.0	0.0462
Week 27	335	30.5	3.9	291	24.3	1.8	0.1067	261	21.8	1.9	0.0263

Figure 1. Study design and tumor analysis of GP supplementation in SKH-1 hairless mice.

(**a**) Analysis report for major GP phytochemical constituents (analyzed by Covance Laboratories, Madison, WI; report provided by CTGC); (**b**) Experimental timeline; (**c**) Representative SKH-1 hairless mice from each group at the end of the study. Location of large tumors is indicated by circles; (**d**) Analysis of tumor multiplicity and numbers for the last 4 weeks. Linear regression is fitted separately for each week, where the model is $Y_i = \mu_0 + \mu_1 I(G_i = 2) + \mu_2 I(G_i = 3) + \varepsilon_i$, where G_i is the group indicator, which equals 1, 2, and 3 for the control, 3% GP, and 5% GP feed groups, respectively, Y_i is the tumor incidence counted at that particular week.

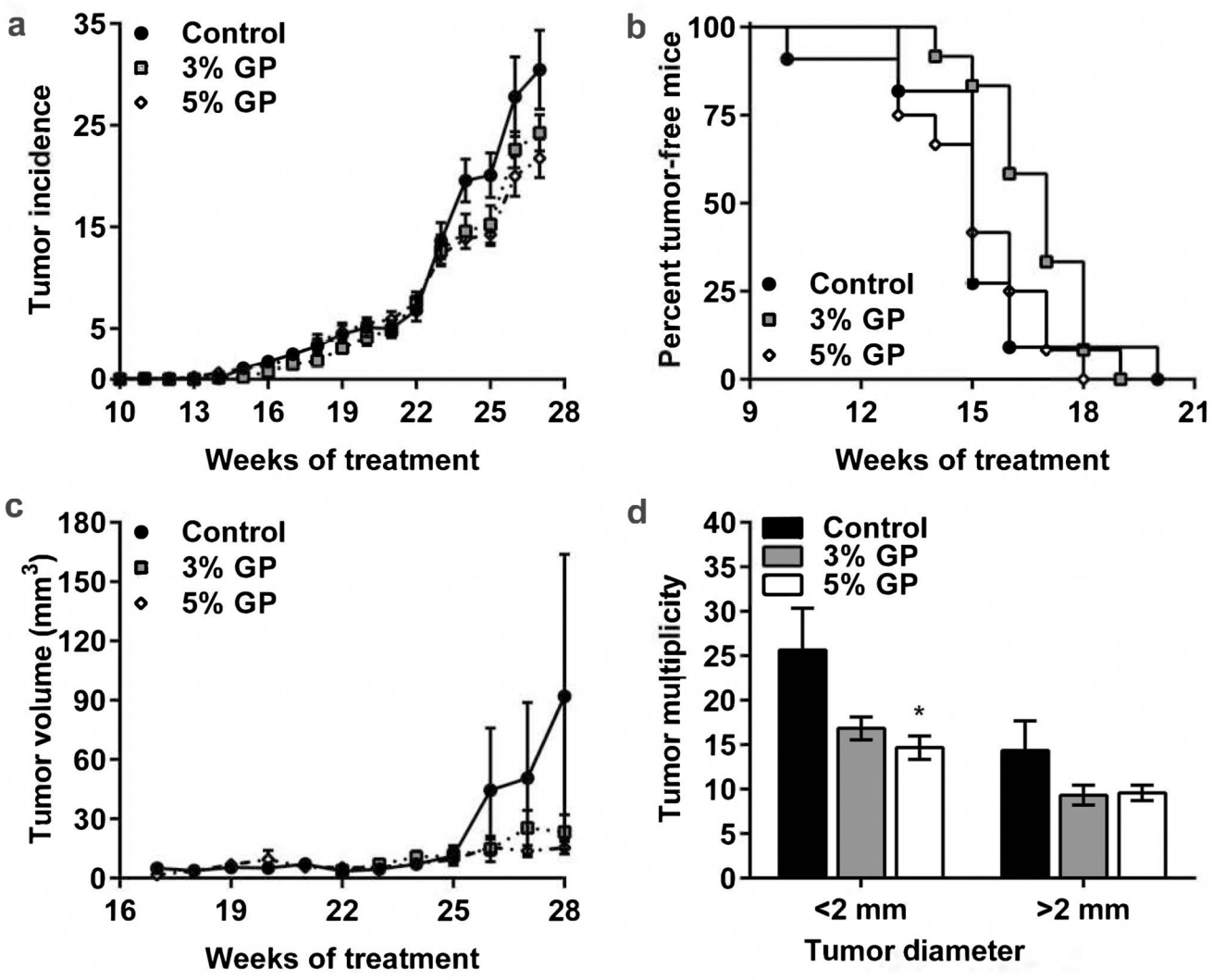

Figure 2. Effect of dietary GP on UVB-mediated skin carcinogenesis in SKH-1 hairless mice.

(**a**) Average tumor incidence per group. Statistical model is described in materials and methods, p-value 0.306 and 0.174 for 3% GP and 5% GP, respectively; (**b**) Kaplan-Meier plot of tumor-free mice, p-values 0.157 and 0.940 for 3% GP and 5% GP, respectively; (**c**) Average tumor volume per group for weeks 16 to 28, p-value 0.352 and 0.455 for 3% GP and 5% GP, respectively; (**d**) Tumor multiplicity at the time of euthanasia. For <2 mm tumors p-value 0.132 and 0.021 for 3% GP and 5% GP, and for >2 mm tumors p-value 0.331 and 0.505 for 3% GP and 5% GP, respectively. All data are presented as mean ± SEM.

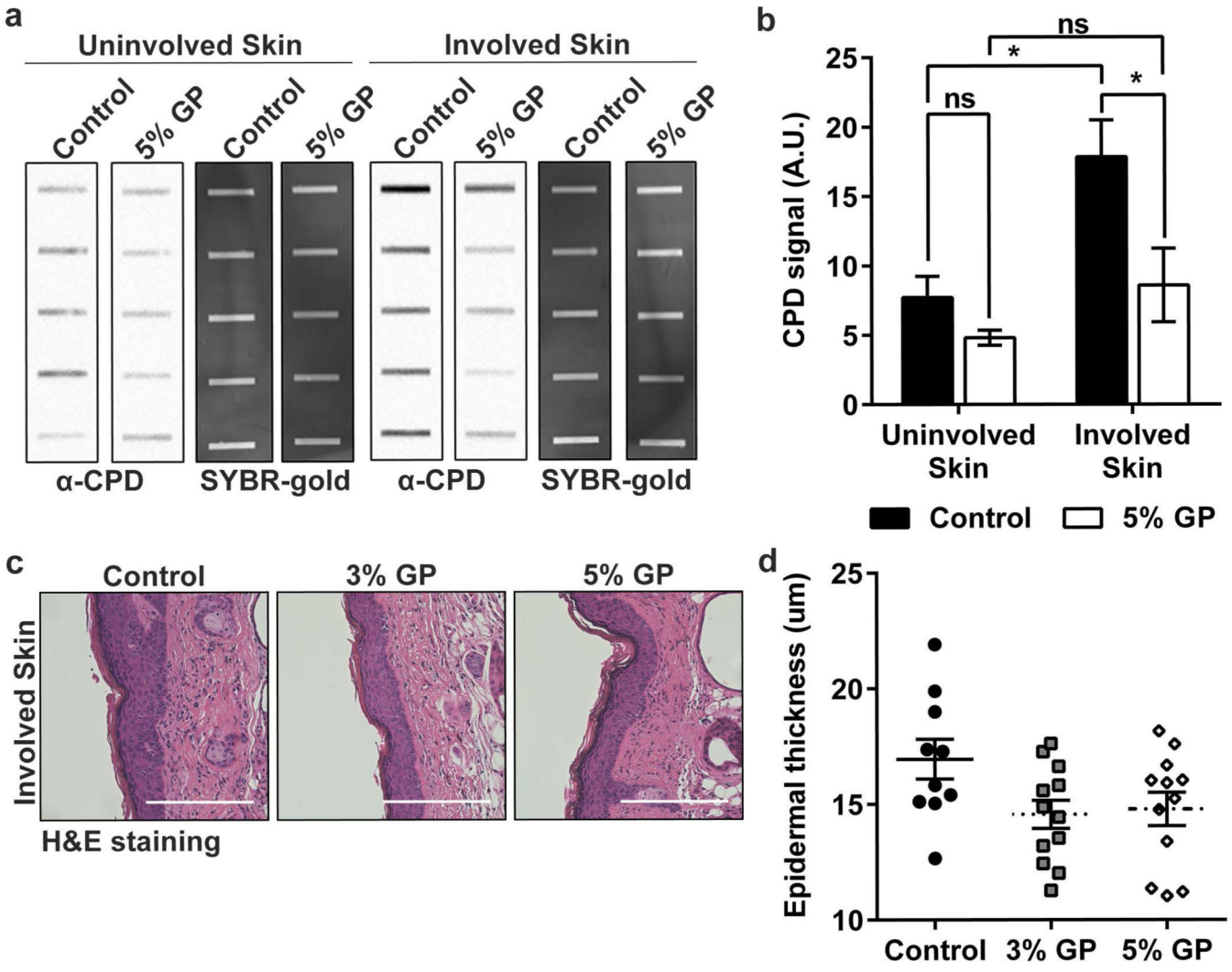

Figure 3. Effect of dietary GP on UVB-induced DNA damages and epidermal thickness.

(**a**) Detection of CPDs in SKH-1 mouse involved (adjacent) and uninvolved (stomach) skin by slot blot following chronic UVB exposure. Each row represents an individual mouse. SYBR gold, which stains total nucleic acid, was used as an internal control; (**b**) Relative quantification of CPD signal from slot blot. AU = arbitrary units, as designated by the imaging software. Statistical analysis was performed using two-way ANOVA with Tukey's multiple comparison. Statistical significance is denoted as *$p<0.05$, ns = no significance; (**c**) Representative images, and (**d**) Quantification of epidermal thickness in skin adjacent to tumors from formalin-fixed, paraffin-embedded tissue sections stained with hematoxylin and eosin (H&E). Images captured at 20x (scale bar = 200 μm). Statistical analysis was performed using one-way ANOVA with Tukey's multiple comparison. p-value 0.072 and 0.111 for 3% GP and 5% GP, respectively All data presented as mean ± SEM.

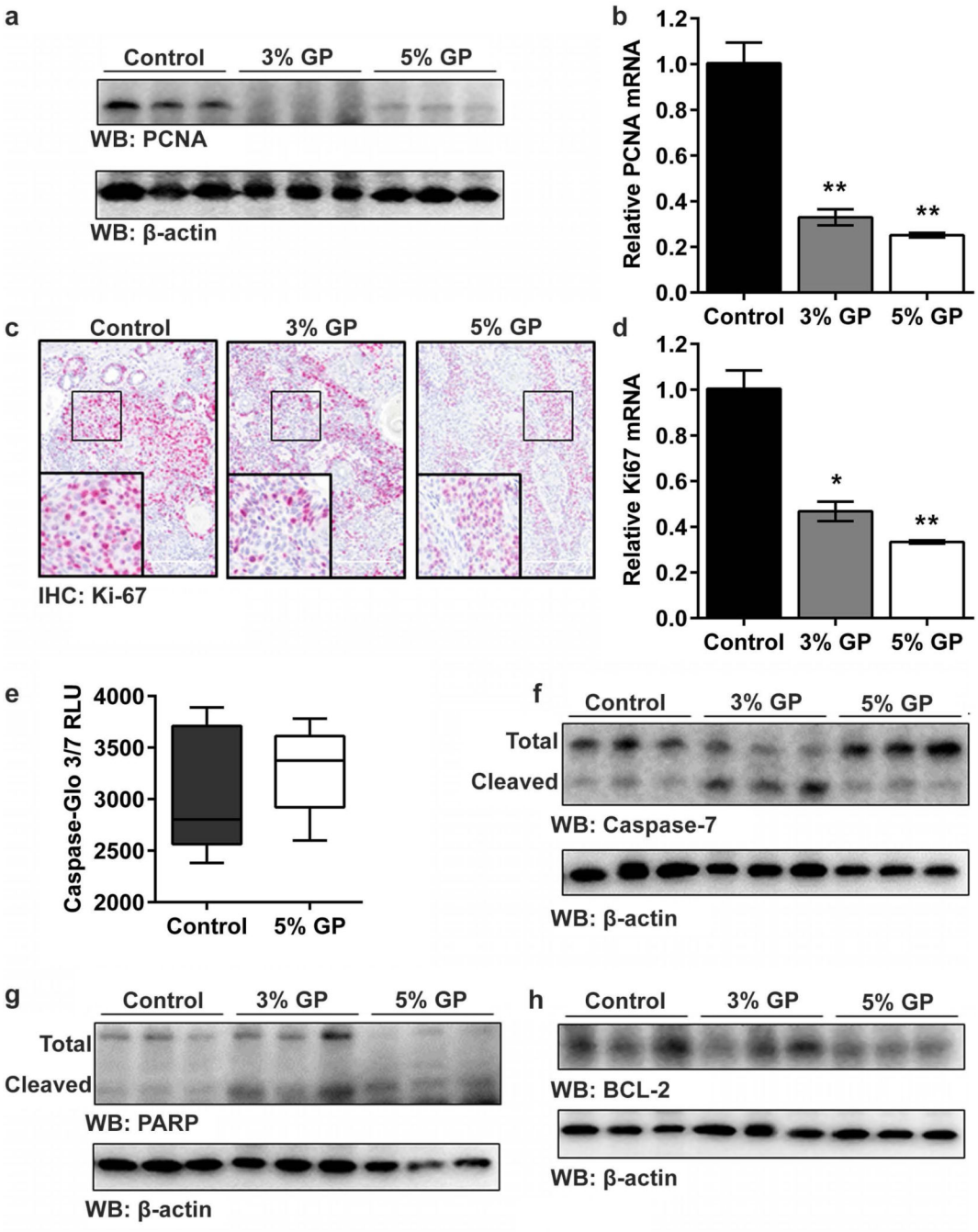

Figure 4. Effect of dietary GP on cell proliferation and apoptosis in UVB-induced tumors.

(**a**) Expression of PCNA protein (by immunoblot), and; (**b**) mRNA (by quantitative real-time reverse transcriptase - PCR (RT-qPCR)); (**c**) Expression of Ki-67 protein (by immunohistochemical staining; 20x magnification; scale bar = 200 μm), and; (**d**) mRNA (by RT-qPCR). Data is presented as mean ± SEM, with statistical analysis performed using one-way ANOVA with Tukey's multiple comparison. Statistical significance denoted as *$p<0.05$ and **$p<0.01$. Effect on (**e**) caspase-3/7 activity, $p=0.061$, and; **(f)** immunoblot analysis of total and cleaved caspase-7; (**g**) immunoblot analysis of total and cleaved PARP; (**h**)

immunoblot analysis of BCL-2 protein. β-actin was used as loading control. RLU = relative intensity unit. Each immunoblot lane represents a pool of three animals as described in materials and methods.

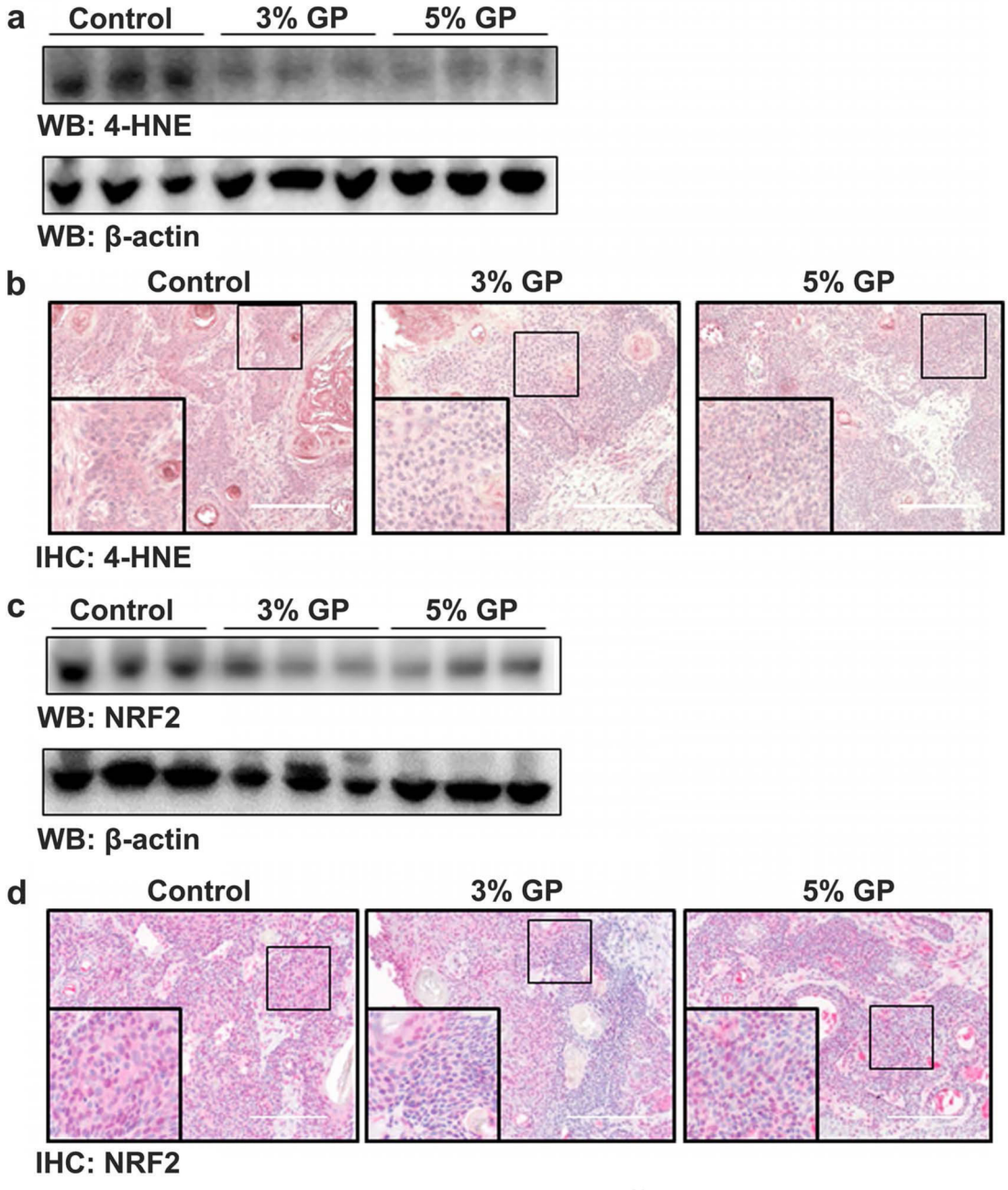

Figure 5. Effect of dietary GP on oxidative stress biomarker 4-HNE and oxidative stress response marker NRF2.

(**a**) Expression of lipid peroxidation marker 4-hydroxynonenal (4-HNE) by immunoblot, and; (**b**) immunohistochemical staining. (**c**) Expression of activator of antioxidant response element, NRF2, by immunoblot, and; (**d**) immunohistochemical staining. Each immunoblot lane represents a pool of three animals as described in materials and methods. A representative image (20× magnification; scale bar = 200 μm) from each group is presented.

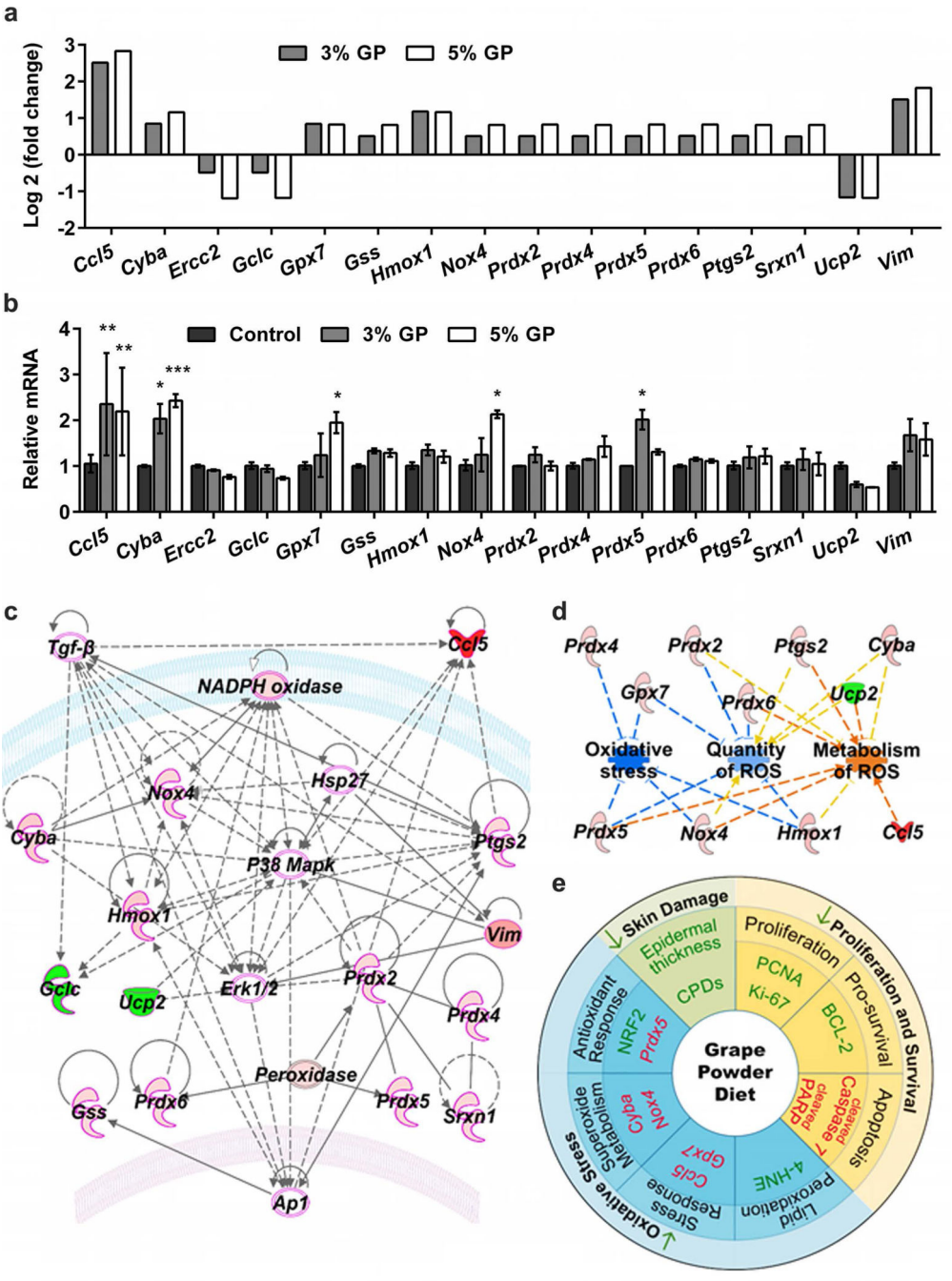

Figure 6. Mechanistic analysis of GP-mediated chemoprotective effects against UVB-induced skin carcinogenesis.

(**a**) Differentially expressed genes in 3 and 5% GP group from the oxidative stress PCR array. Genes with ≥1.75-fold change and $p<0.05$ in response to 5% GP and ≥1.4-fold change in response to 3% GP are included. P-values are calculated based on Student's t-test of the replicate 2^(-ΔCT) values for each gene. (**b**) RT-qPCR validation of key altered genes in response to 3 and 5% GP. The data presented here are from RNA pooled evenly from 9 mouse tumor samples per group as described in materials and methods. Statistical analysis performed using two-way ANOVA with Tukey's multiple comparison. Data are represented

as mean ± SEM (*p<0.05, **p<0.01, ***p<0.001). (**c**) A gene network pathway was generated with key altered genes (≥1.75-fold change in response to 5% GP) using IPA software. Red= upregulated genes; Green= downregulated genes; Pink outline= Cancer-associated genes; Uncolored nodes= genes not included in the PCR array but found during IPA analysis. Gene-gene interactions are indicated by arrows, the solid lines denote a robust correlation with partner genes, and dashed lines indicate statistically significant but less frequent correlations. (**d**) Using IPA, the functional annotations of 5% GP-modulated genes were generated showing inhibition of oxidative stress and quantity of ROS, as well as increased metabolism of ROS. Blue lines= inhibition; Orange= activation; Yellow= findings inconsistent with the state of downstream molecules. (**e**) Schematic representation of the effects of dietary GP on skin tumorigenesis are presented. Green= downregulated/decreased, Red= upregulated/increased measurements.